Carbohydrate Polymers 175 (2017) 207–215

Contents lists available at ScienceDirect

Carbohydrate Polymers

journal homepage: www.elsevier.com/locate/carbpol

A structural study of *Acacia nilotica* and *Acacia modesta* gums

Shazma Massey[a], William MacNaughtan[b,*], Huw E.L. Williams[c], Bettina Wolf[b], Mohammad S. Iqbal[a,*]

[a] Department of Chemistry, Forman Christian College, Lahore 54600, Pakistan
[b] Division of Food Sciences, School of Biosciences, University of Nottingham, Sutton Bonington Campus, Loughborough LE12 5RD, UK
[c] Centre for Biomolecular Sciences, School of Biosciences, University Park, University of Nottingham, NR7 2RD, UK

ARTICLE INFO

Article history:
Received 28 February 2017
Received in revised form 20 July 2017
Accepted 21 July 2017
Available online 24 July 2017

Keywords:
Arabinans
Acacia modesta
Acacia nilotica
Polysaccharides
NMR spectroscopy

ABSTRACT

Superficially similar carbohydrate polymers from similar sources can have dramatically different characteristics. This work seeks to examine the molecular properties responsible for these differences. Protons responsible for cross-polarization in the anomeric region of *Acacia nilotica* (*AN*) were replaced easily by deuterium, but not for *Acacia modesta* (*AM*). Time constants describing the mobility and cross-polarization transfer were both found to be lower for *AM*. Variable contact time experiments showed poorer fits and more heterogeneity for *AN*. Solution state HSQC experiments showed a lower number of environments in the anomeric region for *AM*. The relaxation time T_2 of *AM* solutions had a lower value consistent with a higher viscosity. The T_g' of solutions were −14.5 °C *AN* and −18.5 °C *AM*. These results form a largely self-consistent picture of molecular differences between *AN* and *AM*, suggesting a more compact but heterogeneous structure for *AN* and more branching in the case of *AM*.

1. Introduction

Gum acacia, also known as gum Arabic (E number E 414), is an edible polysaccharide used in the food, pharmaceutical, cosmetic and textile industries, as an emulsifying, suspending and stabilizing agent. *Acacia modesta* (*AM*) and *Acacia nilotica (AN)* are two common varieties of the gum obtained from two species of acacia plant. *AM* gum, also known as gum *Acacia senegal* or gum phulai in South Asia, is the main source of gum Arabic presently used in Industry. This material has been extensively studied and attempts have been made to determine its monosaccharide composition and macromolecular structure using monosaccharide analysis, FT-IR and NMR spectroscopy after hydrolysis of the polymeric materials. Tischer, Gorin, and Iacomini (2002) and Sanchez et al. (2008) reported that acacia gum is a heavily branched polysaccharide containing mainly arabinose and galactose with minimal quantities of rhamnose and other monosaccharides and having a main chain consisting of 1,3 linked β-D-galactopyranosyl units with lesser amounts of α-L-arabinofuranose and other residues, together with a variety of linkages in the side chains including α-D-Gal*p*-(1 → 3)-α-L-Ara*f*, α-L-Ara*f*-(1 → 4)-β-D-Gal*p and* β-D-Gal*p*-(1 → 6)-αβ-D-Gal*p*. It is also defined as a heteropolysaccharide as it contains a significant fraction (above 2%) of polypeptide. Grein et al. (2013) studied the emulsifying properities of a commercial gum Arabic as well as *Acacia mearnsii* de Wild gum and concluded that these were dependent on the structure of the polysaccharide, such as the degree of branching, as well as the protein content and molecular weight of the carbohydrate/protein complexes. Interestingly these authors also noticed a difference in the number of anomeric environments as measured by 2D NMR between the two gums.

On the other hand, very little structural information is available in the literature regarding *AN* gum. *AN* gum, also known as gum kikar in the South Asia, has been reported to possess similar functional properties to *AM*. *AN* gum is available at less than half the price of *AM* gum, and would, therefore, offer a significant saving to industry if the properties were comparable.

AN gum is almost completely, but very slowly, soluble in water and practically insoluble in alcohol. The solution is colorless or yellowish, dense, adhesive and translucent. It has been reported to be a branched-chain polysaccharide containing mainly arabinose and galactose with some uronic acid and trace amounts of rhamnose (Kapoor & Farooqi, 1991). In this study the authors compared 1D ^{13}C NMR spectral patterns of gums obtained from different habitats and did not deal with the spectral assignments in detail. The molar mass of *AN* gum has been reported to range from 0.8×10^6 to 2.3×10^6

* Corresponding authors.
E-mail addresses: shazmaazeem@fccollege.edu.pk (S. Massey), bill.macnaughtan@nottingham.ac.uk (W. MacNaughtan), Huw.Williams@nottingham.ac.uk (H.E.L. Williams), Bettina.Wolf@nottingham.ac.uk (B. Wolf), saeediqbal@fccollege.edu.pk, saeediq50@hotmail.com (M.S. Iqbal).

http://dx.doi.org/10.1016/j.carbpol.2017.07.065

Daltons (Gómez-Díaz, Navaza, & Quintáns-Riveiro, 2008). Physical appearance of the two gums is different; *AN* being of round crystalloid nature and *AM* having the form of L-shaped flexible rods. This fact suggests variation in their secondary structure. Such structural differences can be investigated through a standard set of multidimensional NMR experiments. However, these experiments are difficult to apply to carbohydrates as the chemical environments are so similar that there is often insufficient information to define robust 3D structures. An NMR study as presented here in combination with other techniques, could enable important structural features of the materials to be determined. The structural information may enable the further development of the use of these gums in areas such as the food industry, targeted drug delivery, nanomedicine and tissue engineering.

The hypothesis underpinning this research is that information from a series of techniques including NMR, when considered together can provide useful information concerning structural differences between carbohydrate gums.

2. Experimental

2.1. Materials

AM and *AN* gums were sourced from herbal product shops in local markets in Lahore, Pakistan and purified (procedure available in Supplementary Data). The chemicals and reagents used were: deuterium oxide (PubChem CID: 24602), L-(+)-arabinose (PubChem CID: 439195), D-(+)-galactose (PubChem CID: 6063) and L-rhamnose monohydrate (PubChem CID: 25310) (Sigma-Aldrich, USA); BCA protein assay reagent A and B (cat # 23228 and 23224 respectively, Thermo Scientific, Pierce, USA); and albumin standard (cat # 23209, Thermo Scientific, Pierce, USA). All the chemicals were used without further purification. Distilled water was used throughout this study.

2.2. Analytical and viscosity methods

The monosaccharide analysis procedure and High Performance Liquid Chromatography (HPLC) chromatograms are available in the Supplementary Data. These were performed as reported previously (Massey, Iqbal, Wolf, Mariam, & Rao, 2016). Gel permeation chromatography (GPC) chromatograms are similarly available. These methods show the presence of low levels of other monosaccharides and higher molecular weight materials. The viscosity determinations used a double-gap cylinder geometry (details in Supplementary Data). Over a shear range from 10^{-2} to 10^{4} s^{-1} both polysaccharides showed Newtonian behavior. The viscosity values are low demonstrating that the primary function of these polymers would not be as viscosity enhancers.

2.3. NMR study

NMR spectra were obtained in the solid state (^{13}C cross polarization magic angle spinning, CPMAS) and in solution (multidimensional ^{1}H and ^{13}C). ^{13}C NMR spectra of pure arabinose, galactose, and rhamnose monohydrate, were also recorded in the solid state as references. As the gums were soluble in water 1D and 2D NMR measurements were made in D_2O.

The original protonated material (2.0 g) was dissolved in D_2O (20 mL), freeze-dried, redissolved in D_2O (20 mL), freeze-dried again and finally dissolved in D_2O (20 mL). The original protonated material and the dried deuterated sample after the second freeze-drying stage were used for the solid state NMR measurements.

2.3.1. Solid state experiments

^{13}C CPMAS NMR spectra were recorded on a Bruker AVANCE III 600 NMR spectrometer with narrow bore magnet and 4-mm triple resonance probe. The parameters and conditions used in CPMAS experiments were: proton 90° pulse length 3 μs, field strength of the proton and spin locking fields during the contact period 83 kHz. The samples were packed into 4-mm rotors and spun at 10 kHz. Chemical shifts (ppm) scales were referenced to the upfield peak of adamantane (29.5 ppm) run as an external standard.

Proton decoupling was provided by a Spinal-64 sequence and the proton power levels during the contact time and decoupling stage could be varied independently to provide optimum signal-to-noise levels. The highest intensity signal for all types of bonded carbons in these materials lies between a contact time of 1 and 2 ms. For all CPMAS experiments a value of 2 ms was used. Recycle delay was 2 s.

2.3.2. Variable contact time experiments

Cross-polarization involves the transfer of polarization from proton to carbon for a set period known as the contact time. The carbon signal increases with contact time up to a maximum with the time constant of the increase reflecting the number of protons in the immediate neighborhood of, and distance from the carbon as well as the solidity of the sample. After the maximum signal the decay constant is the proton $T_{1\rho}$ value which gives useful information on the mobility of the system as well as the degree of cross-transfer between protons on various parts of the molecule. By using approximately 15 values of logarithmically spaced contact time, the envelope of the rise and fall of the carbon intensity can be measured and estimates of the decay constants obtained.

2.3.3. Solid state data processing

Approximately 5k of data points were normally recorded. On data processing this data set was zero-filled by at least a factor of 2. A Lorentzian line broadening (15 Hz) was then applied. The data were Fourier-transformed and phased with zero and first order corrections. Baseline fitting routines were applied to all spectra. Mobility measurements were made by integrating defined regions across a series of spectra corresponding to different contact times. The resulting areas were used to obtain optimal decay constants by fitting (Solver, Microsoft Excel®) the area data to the equation:

$$M = I_0/(1\text{-}T_{IS}/T_{1\rho})[\exp(-t/T_{1\rho}) - \exp(-t/T_{IS})] \quad (1)$$

where, I_0 = signal intensity, T_{IS} = time constant of polarization transfer and $T_{1\rho}$ = proton time constant in the rotating frame, reflecting proton mobility

2.3.4. High resolution NMR

All 1D and 2D NMR experiments were carried out on a Bruker 800 MHz Avance III spectrometer equipped with a QCI cryoprobe. For each sample the 90° pulse and transmitter frequency were calibrated. The number of scans collected in each dimension for each experiment was determined by the sample concentration. Data acquisition and processing were carried out using Topspin 3.1 software. The 1D experiments were apodized using an exponential window function with 2 Hz line broadening. For 2D datasets a shifted squared sine bell was used with the offset being optimized to achieve the best balance between resolution and signal-to-noise ratio. All data were zero-filled by at least a factor of 2. For heteronuclear dimensions linear prediction was employed.

2.3.4.1. 1D experiments. The 1D ^{1}H NMR spectra were recorded using a 1D NOESY sequence with a spectral width of 14 ppm using on-resonance presaturation for water suppression. The pro-

ton transmitter frequency was set to 4.702 ppm and typically 64 scans were acquired.

2.3.4.2. 2D experiments. The 2D ^{13}C[H] HSQC spectra were acquired over a spectral width of 14 ppm in the ^{1}H dimension and 200 ppm in the ^{13}C dimension. The transmitter frequency for carbon was centered at 100 ppm and between 16 and 64 scans were acquired, with 128 complex points in f_1. Quadrature detection in the carbon channel was achieved using the States-TPPI method.

2.3.5. Low resolution ^{1}H NMR relaxation

Low resolution ^{1}H NMR was carried out on Resonance Instruments Maran benchtop spectrometer (RI, Oxford UK) operating at 23 MHz. The 90° pulse lengths were approximately 3 μs with recycle delay times of 4 s. T_2 values were determined using a Carr Purcell Gill Meiboom (CPMG) pulse sequence with a τ value of 64 μs and typically 2048 echoes. Data was fitted to single exponential decay curves using Resonance Instruments software. T_1 measurements were made using an inversion recovery pulse sequence with appropriately chosen delay times and used to determine the optimal recycle delay. Measurements were made at a series of dilutions (approximately 40, 20 and 10% solids w/w) and at different temperatures (37, 20 and 4 °C). The NMR measurements were also made on samples dissolved in D_2O resulting in partial replacement of the exchangeable proton fraction and used to estimate the relaxation behavior of the non-exchangeable proton fraction.

2.3.5.1. Form of the relaxation model. A simple combined relaxation and chemical exchange model for protons on the biopolymer and water sites can be described by combining the Bloembergen, Pound Purcell (BPP) (Bloembergen, Purcell, & Pound, 1948) theory with a modified Swift Connick/Carver Richards two site exchange model (Swift & Connick, 1962; Carver & Richards, 1972). Under the limiting conditions of short τ value and low sample concentration the fundamental equation describing exchange reduces to (McConville & Pope, 2001):

$$1/T_{2measured} = (1-P)/T_{2water} + P/(T_{2gum} + \tau_{exchange}) \quad (2)$$

where, P is the gum concentration, $1/\tau_{exchange}$ is the exchange rate (k), and T_{2gum} and T_{2water} are the respective T_2 values for the gum and water. The T_2 values can be predicted by BPP theory according to:

$$1/T_2 = C/2[3\tau_c + 5\tau_c/1+\omega_0{}^2\tau_c{}^2 + 2\tau_c/1+4\omega_0{}^2\tau_c{}^2) \quad (3)$$

where, ω_0 is the spectrometer frequency, τ_c is the correlation time and C is the magnetic dipolar interaction constant. Moreover the dependence of the correlation time (or rate of exchange) on temperature can be assumed to be thermally activated and follow an Arrhenius law as:

$$\tau_c = \tau_0 e^{-(Ea/kT)} \quad (4)$$

Proton densities of water and the carbohydrate gum have been assumed to be 0.111 and 0.062, respectively. It is interesting to note that systems showing predominantly relaxation or exchange behavior exhibit an opposite temperature dependency (Ibbett, Schuster, & Fasching, 2008). T_2 values for the polymer can be crudely estimated from D_2O exchange experiments and from the multi-exponential nature of the decay curve where the initial decay is assumed to be close to non-exchangeable protons on the carbohydrate. An approximate correction has been applied for the fraction of exchangeable protons in the carbohydrate (0.3).

2.4. Differential scanning calorimetry (DSC)

DSC analysis was carried out by heating 40% w/v solutions of the materials at 1 and 5 °C min^{-1} from −50 to +80 °C. Initial cooling from ambient temperature (20 °C) to −50 °C was carried out at a nominal rate of 50 °C min^{-1}. Thermal transitions were monitored using a pre-calibrated heat flux Mettler Toledo DSC 823e (Leicester, UK) equipped with an autosampler and a liquid nitrogen cooling attachment. Samples were hermetically sealed in standard Mettler Toledo 40 uL aluminum pans. Glass transition temperature (T_g) values were calculated using Mettler Toledo Star® software. The T_g' value is the glass transition of the maximally freeze-concentrated state and was assumed to occur at the same temperature as the step observed before the major melting peak of ice. The term T_g refers to a general glass transition.

3. Results and discussion

Yields of the purified gums were approximately 98%. The elemental analysis, FT-IR, monosaccharide analysis, protein analysis and GPC data conformed to those of typical samples of *AN* and *AM* (Massey et al., 2016). Additional chromatographic and viscosity data and methods are included in the Supplementary Data. The molecular mass of the most abundant species measured using light scattering was found to be 1.20×10^6 for *AM*, similar to but slightly greater than the 9.06×10^5 value for *AN*.

3.1. NMR study

The solid state ^{13}C NMR spectra of monosaccharides are shown in Fig. 1a, and the spectra of protonated (original) material and the deuterium exchanged samples are presented in Fig. 1b. ^{1}H NMR spectra of *AM* and *AN* in D_2O are shown in Fig. 2a. HSQC plots for both gums are shown in Fig. 2b and c. A magnified trace shows the superimposed anomeric regions with the complete spectra shown as separate inserts.

3.1.1. Solid state NMR

The CPMAS spectra of the dominant monosaccharides present in the gums exhibit sharp peaks, as all of the chemical environments for each of the particular chemical class of carbons are uniform due to the crystallinity of the materials. Fig. 1b shows that when these sugars are linked in a carbohydrate structure in solid (powder) form, there are many different environments due to different conformations adopted by the sugar units, which produce wider peaks. Fig. 1b also shows that deuterium substitution had a larger effect on *AN* compared with that on *AM*, and changed the peak intensities in the spectrum. In the case of *AN* there are exchangeable protons in close proximity to the corresponding carbons on the sugar units, having chemical shifts at approximately 100 ppm (C1) and 65 ppm (C6) and to a lesser extent in the region 80–90 ppm (C4). These protons are responsible for substantial magnetization transfer in the CPMAS process and hence larger peaks were observed. These have been largely replaced in the partial proton replacement and freeze-drying experiment. This behavior is not seen with *AM* suggesting that there are fairly major differences in the 3D structures of the two materials in the solid state. Whether this structure is carried through to the liquid state is impossible to say from the high resolution experiments presented here. There also appear to be two different chemical shift environments for the carbon in the methyl group of the rhamnose as shown by the double peak in the methyl region. This was also observed in solution.

3.1.2. Mobility of gums in the solid state

Variable contact time plots for the protonated materials are shown in Fig. 3 and the series of decay constants are listed in Table 1. The moisture and D_2O contents of all the four samples were similar. The first observation concerns the poorer fits to Eq. (1) in case of *AN* compared with *AM*. The fit to the early part of the curve is poor

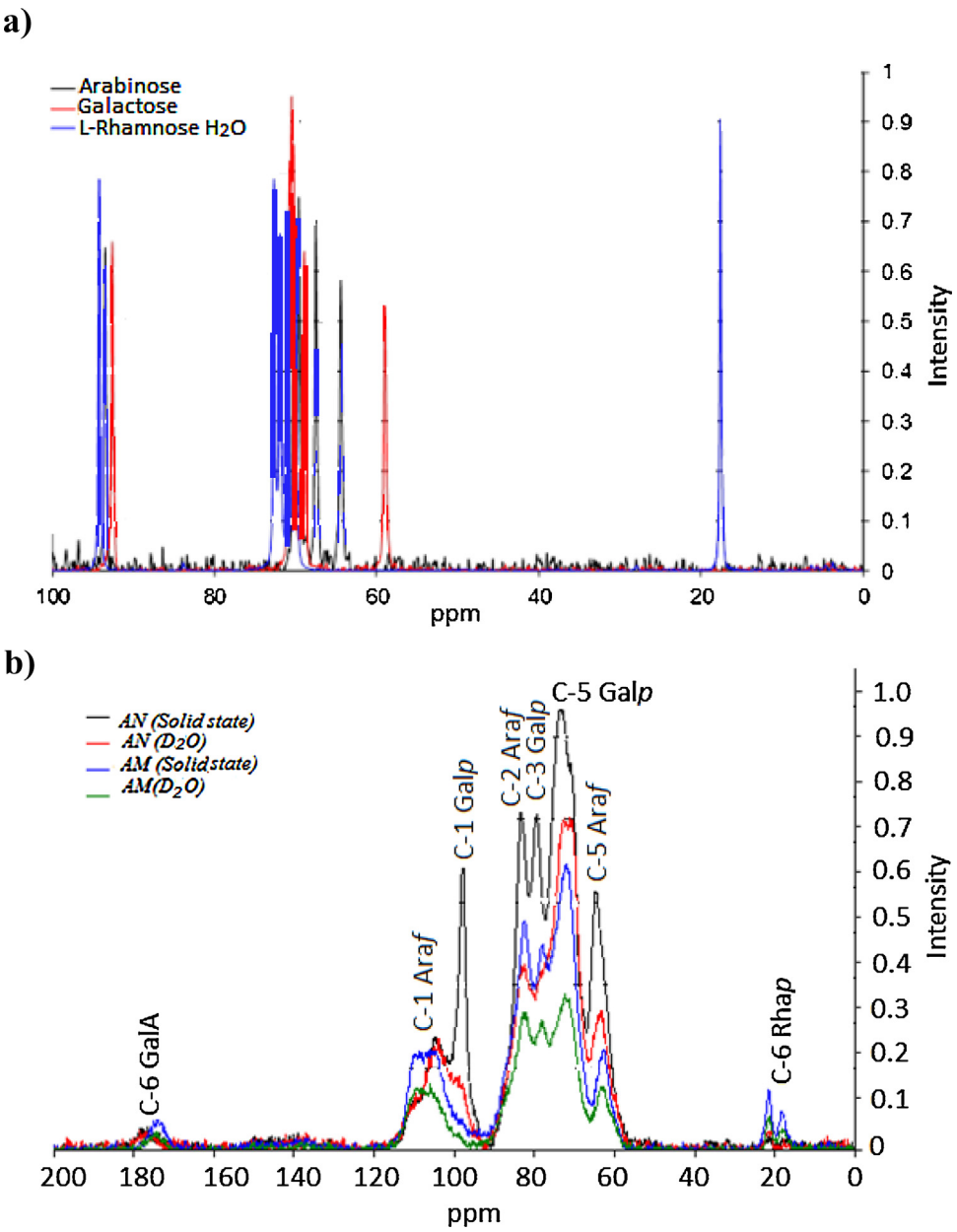

Fig. 1. a) ^{13}C CPMAS spectra of crystalline monosaccharides; b) ^{13}C CPMAS spectra of protonated and D exchanged *AN* and *AM*. Abbreviations A: uronic acid, p: pyranose and *f*: furanose. The intensities are relative.

Table 1
Upper: Solid state variable contact time decay constants T_{IS} and $T_{1\rho}$ and overall intensity I_0 of specified peaks. See also Fig. 3 for fits to most intense peaks. **Lower:** Parameters used for the Relaxation fits in Fig. 4. Water parameters were determined independently using $\tau_0 = 1.4060 \times 10^{-14}$ s and $E_a = 18.2$ kJmol^{-1}.

δ range (ppm)	*AN* untreated			*AN* D_2O-treated			*AM* untreated			*AM* D_2O-treated		
	I_0	T_{IS} (μs)	$T_{1\rho}$ (ms)	I_0	T_{IS} (μs)	$T_{1\rho}$ (ms)	I_0	T_{IS} (μs)	$T_{1\rho}$ (ms)	I_0	T_{IS} (μs)	$T_{1\rho}$ (ms)
165–190	0.035	3043	5.4	0.043	2408	5	0.041	1199	4.5	0.056	2510	2.5
100–120	0.138	109	9.5	0.372	109	9.1	0.287	82	4.6	0.3	77	4.4
90–100	0.162	104	12									
80–90	1.057	96	11.7	0.364	88	8.6	1.114	71	4.8	1.116	69	4.6
65–80				1.058	89	10.5						
50–65	0.244	83	11.2	0.275	67	9.8	0.148	62	3.7	0.173	60	3.5
20–30	0.004	134	1.2	0.012	246	4.1	0.034	195	5.2	0.227	232	4.0
10–20	–	–	–	–	–	–	0.02	195	4.8	0.024	224	3.8

Material	τ_0 untreated polymer (s)	E_a untreated polymer (kJmol^{-1})	τ_0 exchange (s)	E_a exchange (kJmol^{-1})
AN	6.1×10^{-14}	26.4	2.0×10^{-5}	15.9
AM	9.8×10^{-11}	16.3	Low value	–

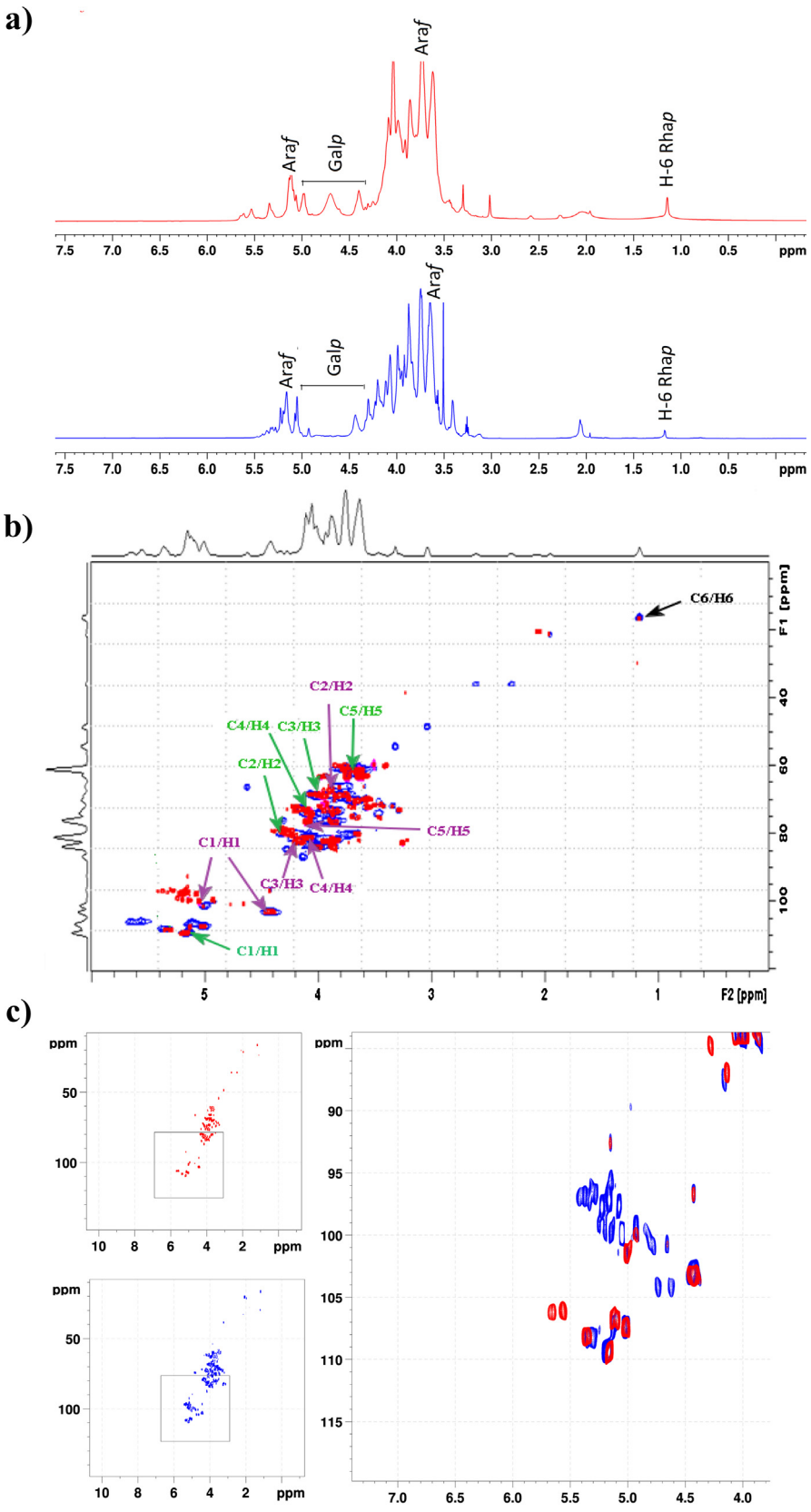

Fig. 2. a) ^{1}H spectra of *AM* (upper) and *AN* (lower) in D_2O. b) HSQC plots (all regions) of *AN* (red) and *AM* (blue). c) HSQC plots of *AN* (blue) and *AM* (red) showing the superimposed anomeric region. (For interpretation of the references to colour in this figure legend, the reader is referred to the web version of this article.)

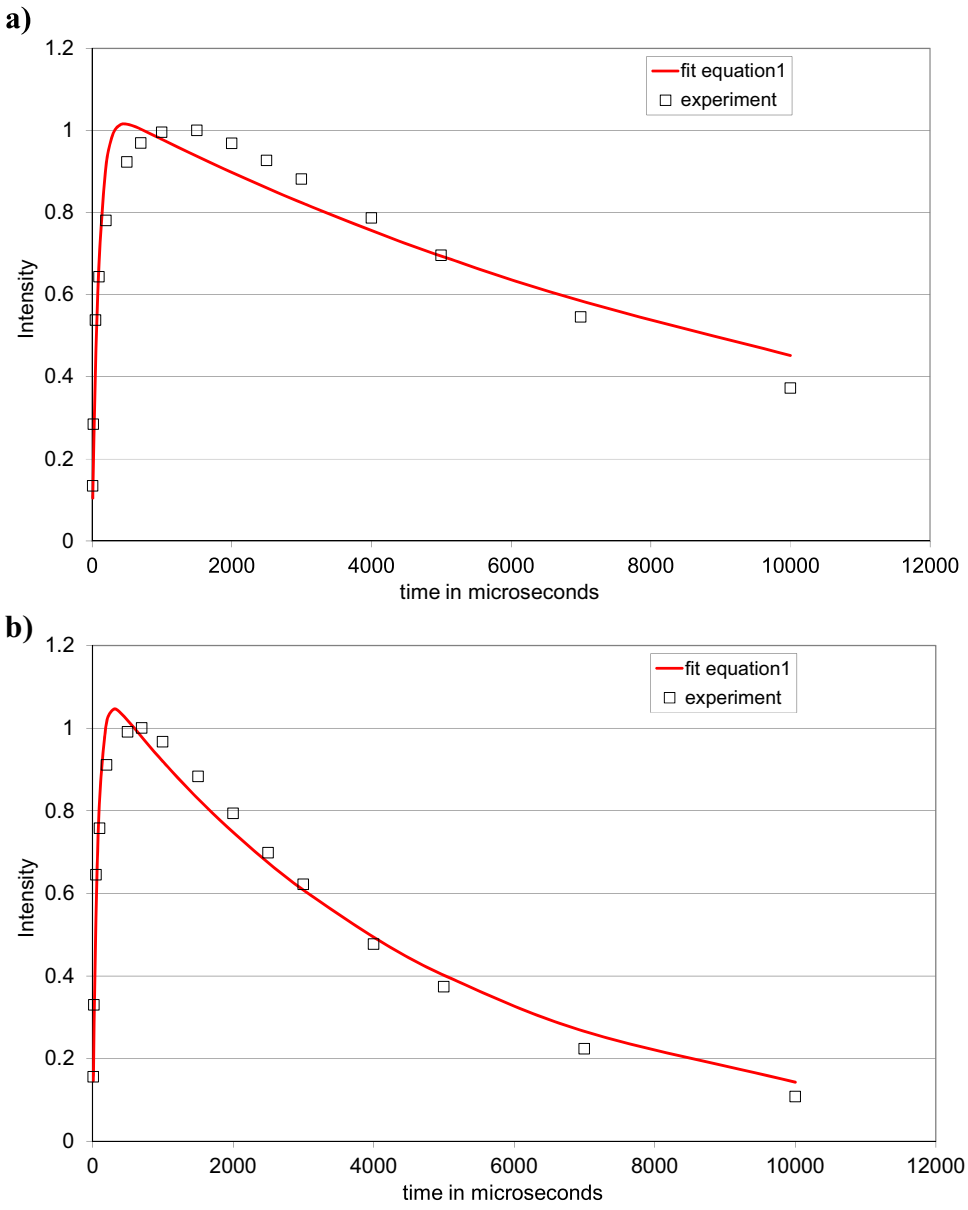

Fig. 3. Quality of fit to Eq. (1), for variable contact time experiments on protonated *AN* (**a**) and *AM* (**b**). The most intense peak, representing a combination of different ring carbons, in the region 65–90 ppm, was selected to demonstrate the fitting procedure.

and any attempt to fit this part better causes a worse fit to the later curve. The complete envelope is better fitted using two (or multi)-component (short and long) T_{IS} decay constants. This suggests that in case of *AN* the structure in the solid state is either less regular in the sense that the protons from other parts of the molecule in the 3D structure seem to be close enough to a carbon atom to transfer magnetization or there is simply much more variation in the structure i.e. more irregularity in the carbohydrate sequence and side groups of the main chain. This produces the multi-component nature of the initial part of the curve. It must be borne in mind that the integration region for the areas used in the fitting encompasses contributions from several carbons which may have different properties and so cause an apparent multicomponent fit. Nevertheless differences are still observed between the two gums and is evidence for heterogeneity in the structure of *AN*.

The other obvious feature of interest is the $H_{T1\rho}$ values. These are uniformly less in case of *AM* as compared with those in *AN* (Fig. 3a and b, Table 1). As these materials are essentially at the same moisture (D_2O or H_2O) content, this implies that there is more mobility in the *AM* spin system. This is perhaps consistent with a more disorganized tangled structure with higher free volume and a polymer having a more branched nature, despite the increased inhomogeneity of *AN* as detected by other properties. Interestingly the 2D NMR also shows broader peaks in case of *AM*.

3.1.3. High resolution NMR

The monosaccharide analysis indicated that *AM* was composed of 68.0% arabinose, 30.0% galactose, and 1.8% rhamnose, while *AN* was composed of 75.0% arabinose and 25.0% galactose (details available in the Supplementary Data). The starting point for the high resolution NMR analysis was the comparison of the two anomeric regions in the HSQC 2D plots for the two polysaccharides together with the identification of any distinct resonances which could be easily assigned to particular sugars such as the carbons in the methyl groups in rhamnopyranose. Broadly speaking chemical shifts greater than 105 ppm indicate the presence of anomeric C1 linked carbons in α-arabinose in the furanose form, whilst shifts less than this primarily indicate the presence of anomeric C1 linked

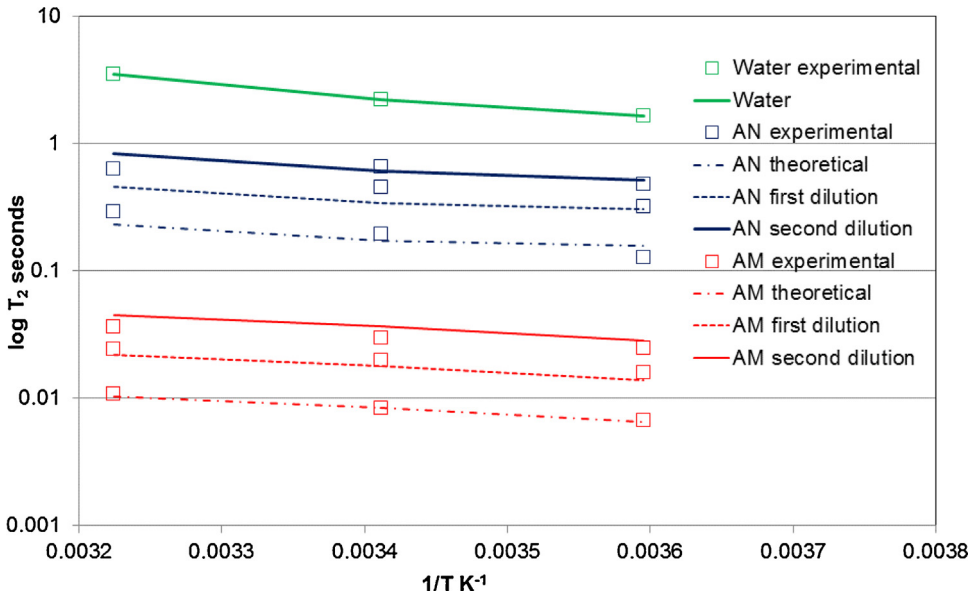

Fig. 4. Fits to the relaxation data. CPMG data with a τ value of 64 μs were used. Fits were optimized over each complete data set using the calculated water and polymer proton concentrations of the dilutions (approximately 40, 20 and 10% polymer). An independent value for the T_2 of water was measured for each temperature and used for optimization.

carbons in β-D-galactopyranose linked residues, as has been found in other carbohydrates (Kang et al., 2011).

In the HSQC plots, each cross peak has carbon and proton coordinates corresponding to the chemical shifts of a ^{13}C and its directly bonded proton. The high-field cross peaks at $\delta = 1.19$ (CH_3) and at $\delta = 17.43$ (CH_3) are consistent with the presence of rhamnopyranose (Rha*p*) units in the polysaccharide (Capeka, Matulováa & Kardošováa, 1997). In the solid state, the ^{13}C signals with low intensities in the region of $\delta = 20$ ppm are due to CH_3 on Rha*p* and those at 175 ppm in *AM* and 178 ppm in *AN* are consistent with a COOH on a galactopyranose (*GalA*). The peaks at $\delta = 20$ ppm are consistent with the monosaccharide analysis, where Rha*p* is present in *AM* (2%) and at very low levels in *AN*.

The appearance of ^{13}C signals due to C-1 and C-5 in arabinose furanose (*Araf*) form at relatively higher δ values than expected for the monosaccharide is consistent with an α-(1,5) linkage of L-arabinose in the main chain (Ochoa-Villarreal, Aispuro-Hernández, Vargas-Arispuro, Martínez-Téllez, & Vargas-Arispuro, 2012). Similarly the appearance of peaks at $\delta = 100.5$ (*AN*) and 103.5 (*AM*) due to the C-1 of Gal*p* and at 80.5 ppm for the C-3 of Gal*p* are consistent with a β-(1,3) linkage of two D-galactose units in the side chain. The carbon resonances in the anomeric regions are well separated, there being approximately 16 in case of *AM* and greater than 32 in the case of *AN*, which gives at least 16 and 32 spin systems for *AM* and *AN* respectively. Peak widths were around 40 Hz for *AM* but sharper (~30 Hz) for *AN*.

The molecular weights of these materials are similar and the viscosity of *AM* is approximately 6 times that of *AN* (0.2 and 0.035 Pa s for *AM* and *AN* respectively), which is also backed up by the proton relaxation T_2 values (Fig. 4) for *AM*, which are substantially lower. *AM* has broader peaks due to the increased viscosity. Since *AM* and *AN* have similar molecular weights, the highly branched structure of *AM* can in part contribute to the higher viscosity and the lower T_2 values observed in the relaxation experiments.

It might be expected that the apparent increased number of anomeric environments for *AN* would be indicative of a more disordered molecule, possibly with increased branching. This has been suggested previously by Grein et al. (2013), however, a lower viscosity was recorded for *AN*, suggesting a more compact structure. The possible presence of lower molecular weight carbohydrates may complicate the NMR interpretation. The presence of small peaks in the HPLC traces (see Supplementary Data S1) indicates that other monosaccharides are present, albeit at a significantly lower concentration than was found in the case of *AM* for rhamnose. The GPC data however suggest the presence of higher molecular-weight materials once again at fairly low levels for both *AN* and *AM*. It is felt that this chromatographic data does not significantly affect the NMR interpretation. In particular the presence of other monosaccharides in the analysis does not account for the possible presence of low molecular-weight material in the HSQC plots.

However there is a group of anomeric peaks in the 5.0–5.5/95–100 ppm $^1H/^{13}C$ range in the HSQC spectrum which is compatible with monosaccharide shifts (Fig. 2b insert). Hence the number of distinct spin systems in the polymeric component of *AN* could be considerably fewer than that of the initial proposed value of greater than 32. An alternative explanation for the higher number of spin systems would be a more heterogeneous structure, i.e., more chemical environments, but nevertheless a maintenance of a compact structure with little branching. Increased heterogeneity and compact structure are not necessarily mutually exclusive.

The ^1H NMR spectra were complex and proton splitting patterns were not easy to distinguish. Broadly, assignments were made by comparing the spectra with those reported for similar materials (Bubb, 2006; Fischer et al., 2004; Carek, Kardosova, & Lath, 1999; Capeka et al., 1997; Ochoa-Villarreal et al., 2012; Saghir, Iqbal, Hussain, Koschella, & Heinze, 2008; Westphal et al., 2010). The anomeric proton signals were well resolved and appeared at $\delta = 5.27$ ppm due to H-1 of Rha*p*, $\delta = 5.16$ ppm due to H-1 of Ara*f*, $\delta = 5.05$ ppm due to H-1 of Gal*p* and $\delta = 4.40$ ppm due to H-2 of Ara*f*. The CH_3 (on C-6 of Rha*p*) signal was observed at $\delta = 1.19$ ppm (Carek et al., 1999).

3.1.4. Relaxation NMR

According to the model presented here the exchangeable protons on the polymers are in exchange with those in water. Arrhenius parameters corresponding to Eq. (4) are shown in Table 1 and the fits shown in Fig. 4. There being no major transitions in the region 5–80 °C and no unusual behavior of the gum solutions, a simple interpretation of the data, unlike some analyses previously reported (Williams et al., 2000; Zhang, Nishinari, Williams, Foster, &

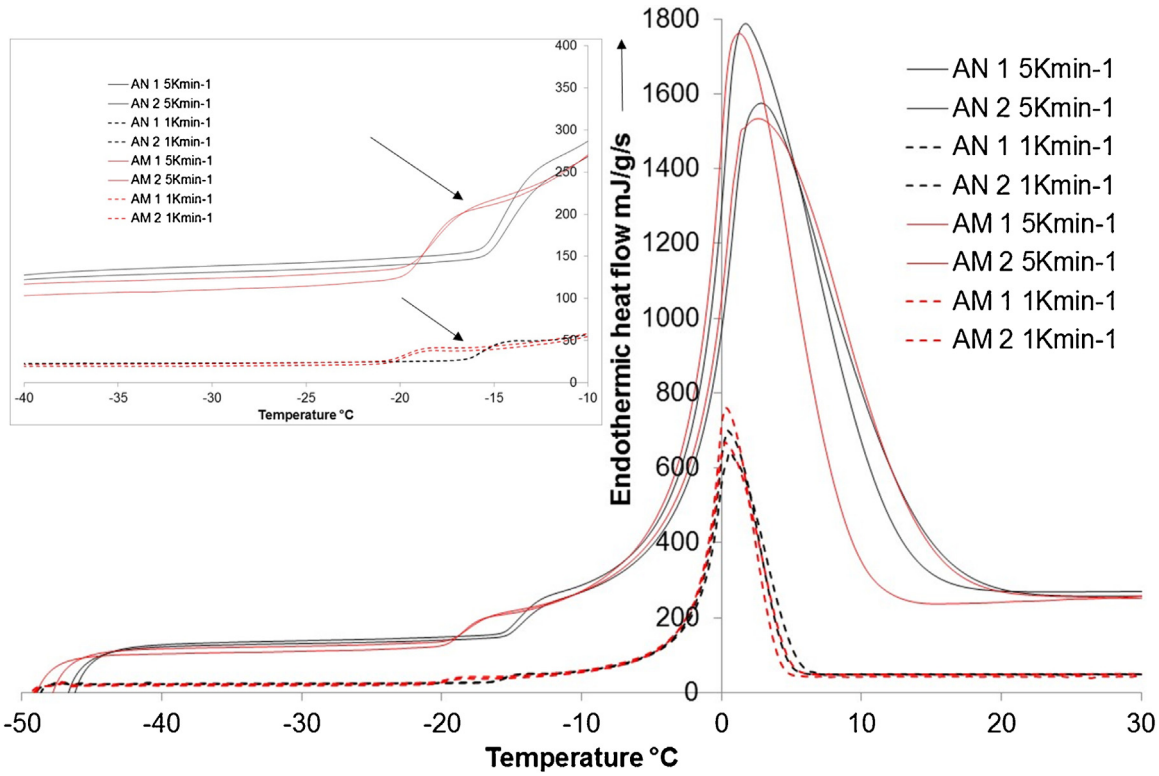

Fig. 5. DSC traces for 40% solutions of *AN* and *AM* heated at a rate of 1 °C min^{-1} (lower 4 traces) and 5 °C min^{-1} showing the complete transitions including the large peak around 0 °C due to ice melting. Samples were cooled initially from room temperature to −50 °C at a rate of 50 °C min^{-1}. An expanded trace is shown on the insert, of the T_g' and onset of ice melting region. Repeat runs are shown.

Norton, 2002) is possible. The rather poor agreement between theoretical fits and measured relaxations, particularly for *AM*, is due to inadequacies of the model and probably not due to any error in the estimation of proton concentration. It may be, for example, due to inaccessibility of exchangeable protons and consequent effective reduction of the proton concentration. The values for the Arrhenius parameter (Table 1) are not robust, as for each polysaccharide, four parameters were varied (parameters for the water being measured independently).

It is possible to measure approximate independent T_2 values from initial rapid decays sometimes observed in a CPMG experiment at small values of τ. Alternatively the gum can be dissolved in deuterium oxide and although not completely replacing all the protons on exchangeable sites, a better estimate of rotational mobility T_2 of the polymer molecules themselves can be obtained. By independently fixing the T_2 value for the polymer, a more robust estimate of the fitting parameters, albeit with a poorer overall fit, can be obtained. The main result from these experiments is the dramatically lower T_2 value for *AM* compared with *AN* solutions, which is primarily due to the approximately 6 × increased viscosity. Bearing in mind the reciprocal relationship between the exchange rate constant and the time constant for exchange, the low values of $\tau_{exchange}$ on Table 1 suggest that there is a high exchange rate constant in the case of *AM*. The higher values for $\tau_{exchange}$ in case of *AN* could be due to a concentration effect, such as the lower accessibility of the protons in the case of the closed structure of *AN* compared with the branched and more open structure of *AM*. Alternatively there could simply be less effective exchange between the protons of water and the polysaccharide in case of *AN*. In fact the poor fit in the case of *AM* suggests there may have been an overestimate of the T_2 value for the polymer. The conclusion from the relaxation work is that changes in the mobility of the polymer *AM*, possibly due to a more branched structure, is reflected in the overall measured reduction in the value of T_2.

3.2. DSC analysis

The DSC curves for *AN* and *AM* are shown in Fig. 5. These curves provide controversial information regarding the glass transition T_g' of the maximally freeze-concentrated state. It has been suggested that smaller molecules should have lower T_g' values, both in the dry and maximally freeze-concentrated state, than larger molecules (MacNaughtan & Farhat, 2008). The values obtained in the present work, −14.5 °C (*AN*) and −18.5 °C (*AM*) both calculated from the scans at 5 °C min^{-1}, appear to contradict this as the other data presented here indicated that the molecular mass of *AM* was similar to and perhaps greater than that of *AN* depending on the exact method of measurement. In addition, there appears to be no indication of non-equilibrium behavior which can distort the heating curves and result in misleading values for the true value of T_g' (Ablett, Izzard, & Lillford, 1992). Although T_g' and non-equilibrium transitions can have very low temperatures for small carbohydrates such as glucose, transitions for larger molecules such as the polymers used here have higher values and there is no indication on the traces of any low temperature transition or indeed the high temperature end of any transition which would indicate non-equilibrium behavior occurring on the traces. The values of T_g' are close although significantly different, however relatively small differences such as these can have a large effects on processing and stability in the foods area. With regard to the effect of molecular weight, larger differences might be expected if the T_g values of dry non-hydrated materials were considered due to the shape of the state diagram. Probably neither the T_g nor the T_g' give definitive structural information but the T_g' values merely suggest here that factors other than molecular weight determine the value.

No evidence of thermal transitions in the higher temperature region of 0–80 °C was found, as is commonly observed in solutions of other biopolymers such as xanthan. There appear to be factors other than molecular weight or thermal transitions in the

gum polymers themselves which contribute to these results. The steps observed in the DSC traces (arrowed on Fig. 5) have been suggested to be the T_g' of the maximally concentrated phase despite the unreasonably large value of the step in heat capacity ΔCp (Slade & Levine, 1991) — a step greater than that for the glass transition of a typical carbohydrate. The larger than expected heat capacity change has been proposed to be predominantly associated with the onset of the melting of the ice fraction (Ablett, Clark, Izzard, & Lillford, 1992). In some non-equilibrium situations the T_g (non-maximally freeze concentrated) and the onset of ice melting may be completely dissociated. Models have been constructed previously in hydrogels and carbohydrate polymeric materials, which suggest that the structure and in particular the effective pore size of the gel/viscous solution, as well as the strength of the carbohydrate main chains can affect the temperature of onset of the formation of ice (Muhr, 1983) and by implication the lowest temperature of final formation of the ice fraction. It is speculated that the more branched structure of *AM*, presumably having reduced effective pore size due to an entangled structure, will reduce the temperature of the onset of ice formation and that the temperature of the step is, therefore, not solely dependent on the molecular mass and indeed may not reflect a true glass transition of the maximally concentrated phase at all. This cryoprotectant property of the *AM* gum may be of use in the formulation of low temperature structures in frozen foods.

4. Conclusions

This study has highlighted structural differences between water soluble *AM* and *AN* gums. The differences in properties of the gums observed in this work are attributed to differences in structure rather than in molecular mass. *AN* was more heterogeneous at a chemical level but had a more compact structure in contrast to the more branched structure of *AM*. The following observations have enabled these conclusions to be drawn. *AM* had a similar but slightly higher molecular mass together with a higher viscosity and lower T_2 values in solution. CPMAS NMR measurements on dry powders showed higher mobility for *AM* and more difficulty fitting variable contact time experiments for *AN* suggesting more heterogeneity for the latter. 2D NMR measurements in solution showed more local environments for anomeric carbons of *AN*. DSC measurements showed higher values for the glass transition temperature of the maximally freeze-concentrated phase and the onset of ice melting for *AN*. The apparent lowering of the temperature of the maximally freeze-concentrated glass in the case of AM gives an additional perspective to the use of these materials in the formulation of foods and drug delivery devices. Moreover the structural differences indicate that the two varieties of the gum may not be used interchangeably in various applications.

Acknowledgements

Shazma Massey acknowledges a research grant from HEC Pakistan (No. 20-3775/NRPU/R&D/HEC/14/1220) and a study leave by Forman Christian College Lahore, Pakistan for making the research possible at University of Nottingham, UK. The authors are thankful to Dr David Coles, School of Biosciences, University of Nottingham, UK, for carrying out the monosaccharide analysis.

Appendix A. Supplementary data

Supplementary data associated with this article can be found, in the online version, at http://dx.doi.org/10.1016/j.carbpol.2017.07.065.

References

Ablett, S., Clark, A. H., Izzard, M. J., & Lillford, P. J. (1992). Modelling of heat capacity–temperature data for sucrose–water systems. *Journal of the Chemical Society, Faraday Transactions*, *88*, 795–802.
Ablett, S., Izzard, M. J., & Lillford, P. J. (1992). Differential scanning calorimetric study of frozen sucrose and glycerol solutions. *Journal of the Chemical Society, Faraday Transactions*, *88*(6), 789–794.
Bloembergen, N., Purcell, E. M., & Pound, R. V. (1948). Relaxation effects in nuclear magnetic resonance absorption. *Physical Review*, *73*(7), 679.
Bubb, W. A. (2006). *NMR Spectroscopy in the study of carbohydrates: Characterizing the structural complexity. School of Molecular and Microbial Biosciences*. New South wales, Australia: University of Sydney.
Capeka, P., Matulováa, M., & Kardošováa, A. (1997). An acidic heteropolysaccharide from the flowers of malva mauritiana l. *Journal of Carbohydrate Chemistry*, *16*(9), 1373–1391.
Carek, P., Kardosova, A., & Lath, D. (1999). A neutral heteropolysaccharide from the flowers of *Malva mauritiana* L. *Chemical Papers*, *53*(20), 131–136.
Carver, J. P., & Richards, R. E. (1972). A general two-site solution for the chemical exchange produced dependence of T2 upon the carr-Purcell pulse separation. *Journal of Magnetic Resonance (1969)*, *6*(1), 89–105.
Fischer, M. H., Yu, N., Gray, G. R., Ralph, J., Andersond, L., & Marletta, J. A. (2004). The gel-forming polysaccharide of psyllium husk (Plantago ovata Forsk). *Carbohydrate Research*, *339*, 2009–2017.
Gómez-Díaz, D., Navaza, J. M., & Quintáns-Riveiro, L. C. (2008). Intrinsic viscosity and flow behavior of Arabic gum aqueous solutions. *International Journal of Food Properties*, *11*, 773–780.
Grein, A., da Silva, B. C., Wendel, C. F., Tischer, C. A., Sierakowski, M. R., Moura, A. B. D., et al. (2013). Structural characterization and emulsifying properties of polysaccharides of *Acacia mearnsii* de Wild gum. *Carbohydrate Polymers*, *92*, 312–320.
Ibbett, R. N., Schuster, K. C., & Fasching, M. (2008). The study of water behaviour in regenerated cellulosic fibres by low-resolution proton NMR. *Polymer*, *49*(23), 5013–5022.
Kang, J., Cui, S. W., Phillips, G. O., Chen, J., Guo, Q., & Wang, Q. (2011). New studies on gum ghatti (Anogeissus latifolia) part II. Structure characterization of an arabinogalactan from the gum by 1D, 2D NMR spectroscopy and methylation analysis. *Food Hydrocolloids*, *25*(8), 1991–1998.
Kapoor, V. P., & Farooqi, M. I. H. (1991). Studies on Acacia nilotica gum exudates. structural variation due to different habitats. *Carbohydrate Research*, *222*, 289–293.
MacNaughtan, W., & Farhat, I. A. (2008). Chapter 9 in Principles and applications of thermal analysis. In P. Gabbott (Ed.),. John Wiley & Sons.
Massey, S., Iqbal, M. S., Wolf, B., Mariam, I., & Rao, S. (2016). Comparative drug loading and release study on some carbohydrate polymers. *Latin American Journal of Pharmacy*, *35*(1), 146–155.
McConville, P., & Pope, J. (2001). H-1 NMR T-2 relaxation in contact lens hydrogels as a probe of water mobility. *Polymer*, *42*(8), 3559–3568.
Muhr, A. (1983). *The influence of polysaccharides on ice formation in sucrose solutions. Diss*. University of Nottingham.
Ochoa-Villarreal, M., Aispuro-Hernández, E., Vargus-Arispuro, I., Martínez-Téllez, M. Á. M., & Vargas-Arispuro, I. (2012). *Plant cell wall polymers: Function, structure and biological activity of their derivatives*.
Saghir, S., Iqbal, M. S., Hussain, M. A., Koschella, A., & Heinze, T. (2008). Structure characterization and carboxymethylation of arabinoxylan isolated from Ispaghula (Plantago ovata) seed husk. *Carbohydrate Polymers*, *74*, 309–317.
Sanchez, C., Schmitt, C., Kolodziejczyk, E., Lapp, A., Gaillard, C., & Renard, D. (2008). The acacia gum arabinogalactan fraction is a thin oblate ellipsoid: A new model based on small-angle neutron scattering and ab initio calculation. *Biophysical Journal*, *94*(2), 629–639.
Slade, L., & Levine, H. (1991). Beyond water activity: Recent advances based on an alternative approach to the assessment of food quality and safety. *Critical Reviews in Food Science and Nutrition*, *30*, 115.
Swift, T. J., & Connick, R. E. (1962). NMR relaxation mechanisms of O17 in aqueous solutions of paramagnetic cations and the lifetime of water molecules in the first coordination sphere. *The Journal of Chemical Physics*, *37*(2), 307–320.
Tischer, C. A., Gorin, P. A. J., & Iacomini, M. (2002). The free reducing oligosaccharides of gum Arabic: Aids for structural assignments in the polysaccharide. *Carbohydrate Polymers*, *47*, 151–158.
Westphal, Y., Kühnel, S., Waard, P. D., Hinz, S. W. A., Schols, H. A., Voragen, A. G. J., et al. (2010). Branched arabino-oligosaccharides isolated from sugar beet arabinan. *Carbohydrate Research*, *345*(9), 1180–1189.
Williams, M. A. K., Foster, T. J., Martin, D. R., Norton, I. T., Yoshimura, M., & Nishinari, K. (2000). A molecular description of the gelation mechanism of konjac mannan. *Biomacromolecules*, *1*(3), 440–450.
Zhang, H., Nishinari, K., Williams, M. A. K., Foster, T. J., & Norton, I. T. (2002). A molecular description of the gelation mechanism of curdlan. *International Journal of Biological Macromolecules*, *30*(1), 7–16.